

assessed its pathogenicity in hACE2 mice. We found that the GX_P2V(short_3UTR) clone can infect hACE2 mice, with high viral loads detected in both lung and brain tissues. This infection resulted in 100% mortality in the hACE2 mice. We surmise that the cause of death may be linked to the occurrence of late brain infection.

The GX_P2V(short_3UTR) mutant, initially isolated from the early passages of the GX_P2V sample (6), and the GX_P2V virus itself, have not been studied in terms of their adaptive mutations in cell cultures. To obtain a genetically homogenous clone for animal experiments, we cloned the passaged mutant through two successive plaque assays. Eight viral clones were chosen for next-generation sequencing (National Genomics Data Center of China, GSA: CRA014225). These clones, when compared with the genome of the original mutant (6), all shared four identical mutations: ORF1ab_D6889G, S_T730I, S_K807N, and E_A22D (Supporting Information, Table S1). Clone 7, named as GX_P2V C7, was randomly selected for the evaluation of viral pathogenicity in hACE2 mice (Figure 1A). The hACE2 mouse model expressing human ACE2 under control of the CAG promoter was developed using random integration technology by Beijing SpePharm Biotechnology Company.

We initially assessed whether GX_P2V C7 could cause disease in hACE2 mice by monitoring daily weight and clinical symptoms. A total of four 6 to 8-week-old hACE2 mice were intranasally infected with a dosage of 5×10^5 plaque-forming units (pfu) of the virus. Four mice inoculated with inactivated virus and four mock-infected mice were used as controls. Surprisingly, all the mice that were infected with the live virus succumbed to the infection within 7-8 days post-inoculation, rendering a mortality rate

of 100% (Figure 1B). The mice began to exhibit a decrease in body weight starting from day 5 post-infection, reaching a 10% decrease from the initial weight by day 6 (Figure 1C). By the seventh day following infection, the mice displayed symptoms such as piloerection, hunched posture, and sluggish movements, and their eyes turned white. The criteria for clinical scoring of the mice and the daily clinical scores post-infection with GX_P2V C7 are provided in the Supporting Information, Figure S1.

We then evaluated the tissue tropism of GX_P2V C7 in hACE2 mice. Using the infection method described above, eight hACE2 mice were infected, eight mice were inoculated with inactivated virus, and another eight mock-infected mice were used as controls. The organs of four randomly selected mice in each group were dissected on days 3 and 6 post-infection for quantitative analysis of viral RNA and titer. We detected significant amounts of viral RNA in the brain, lung, turbinate, eye, and trachea of the GX_P2V C7 infected mice (Figure 1D), whereas no or a low amount of viral RNA was detected in other organs such as the heart, liver, spleen, kidneys, tongue, stomach, and intestines. Specifically, in lung samples, we detected high viral RNA loads on days 3 and 6 post-infection, with no significant difference between these two time points (~ 6.3 versus ~ 5.8 $\text{Log}_{10}[\text{copies/mg}]$). In brain samples, on day 3 post-infection, viral RNA was detected in all four infected mice, with an average value of 5.4 $\text{Log}_{10}[\text{copies/mg}]$. Notably, by day 6 post-infection, we detected exceptionally high viral RNA loads (~ 8.5 $\text{Log}_{10}[\text{copies/mg}]$) in the brain samples from all four infected mice (Figure 1D). On days 3 and 6 post-infection, the viral RNA loads in the turbinate were similar, approximately 4.1 and 3.9 $\text{Log}_{10}[\text{copies/mg}]$, respectively. The viral RNA

loads in the trachea and eyes of the mice surpassed the limit of detection only on day 6 post-infection, with values of 2.6 and 3.8 Log₁₀[copies/mg], respectively. Regarding the infectious viral titers, lung tissues at day 3 post-infection had a value of ~ 1.8 Log₁₀[pfu/mg], which decreased to ~ 0.5 Log₁₀[pfu/mg] by day 6. Importantly, the highest infectious titers were detected in the brain on day 6, which was significantly greater than that on day 3 (~ 0.9 vs ~ 4.8 Log₁₀[pfu/mg]) (Figure 1E). Additionally, there were no significant differences in the infectious titers in the turbinate between day 3 (~ 0.9 Log₁₀[pfu/mg]) and day 6 (~ 1.2 Log₁₀[pfu/mg]) (Figure 1E). By day 6, approximately 2.0 Log₁₀[pfu/mg] was detected in the eyes of two mice. Neither inactivated GX_P2V C7 nor mock infection caused death or any clinical symptoms in the mice (Figure 1B-C and Supporting Information, Figure S2). In summary, in the mice infected with live virus, the viral load in the lungs significantly decreased by day 6; both the viral RNA loads and viral titers in the brain samples were relatively low on day 3, but substantially increased by day 6. This finding suggested that severe brain infection during the later stages of infection may be the key cause of death in these mice.

To determine the mechanisms underlying GX_P2V C7-induced death in hACE2 mice, we examined the pathological changes, presence of viral antigens, and cytokine profiles in the lung and brain tissues of the mice on days 3 and 6 post-infection (Figure 1F-G, and Supporting Information, Figure S3 and S4). On both days, compared to those of control mice, the lungs of infected mice showed no significant pathological alterations, with only minor inflammatory responses due to slight granulocyte infiltration (Figure 1F). On day 3 post-infection, shrunken neurons were visible in the

cerebral cortex of the mice. By day 6, in addition to the shrunken neurons, there was focal lymphocytic infiltration around the blood vessels, although no conspicuous inflammatory reaction was observed (Figure 1G). Upon staining for viral nucleocapsid protein via immunohistochemistry, viral antigens were detected in both the lungs and brains on days 3 and 6 post-infection, with extensive viral antigens notably present in the brain on day 6 (Figure 1F-G). These findings align with the viral RNA load assessments in the lung and brain tissues (Figure 1D). We also performed a Luminex cytokine assay to detect 31 cytokines/chemokines in the lung and brain tissues of the mice (Supporting Information, Figure S3 and S4). Consistent with the pathological findings, there were slight increases or decreases in the levels of many cytokines/chemokines in lung and brain tissues compared to those in control tissues, but the levels of key inflammatory factors, such as IFN- γ , IL-6, IL-1 β , and TNF- α , did not significantly change. In brief, these analyses revealed that GX_P2V C7 infection in hACE2 mice did not lead to severe inflammatory reactions, a finding that aligns with previous reports by Zhengli Shi's group using GX_P2V infection in two different hACE2 mouse models (5), as well as our own findings in the golden hamster model (6).

To the best of our knowledge, this is the first report showing that a SARS-CoV-2-related pangolin coronavirus can cause 100% mortality in hACE2 mice, suggesting a risk for GX_P2V to spill over into humans. Our findings are evidently inconsistent with those of Zhengli Shi *et al.* (5), who tested the virulence of GX_P2V in two different hACE2 mouse models. It is important to note that we did not isolate the wild-type GX_P2V strain. The study by Zhengli Shi *et al* tested the GX_P2V(short_3UTR)

variant that we reported. However, the adaptative evolutionary changes of this variant during their laboratory culture remain understudied. In fact, according to additional infection experiments, the uncloned GX_P2V(short_3UTR) also resulted in 100% mortality in hACE2 mice. Due to the propensity of coronaviruses to undergo adaptive mutation during passage culture, we cloned and analyzed mutations in GX_P2V(short_3UTR), focusing specifically on the pathogenicity of the cloned strains. The high pathogenicity mechanism of GX_P2V C7 in hACE2 mice, in the absence of the wild-type GX_P2V control, requires further investigation. Compared to the original sequence of GX_P2V(short_3UTR), GX_P2V C7 has two amino acid mutations in the spike protein. Given the close relationship between coronavirus virulence and spike protein mutations (7), it is possible that GX_P2V C7 has undergone a virulence-enhancing mutation. However, it is important to note that our hACE2 mouse model may be relatively unique. The company has not yet published a paper on this hACE2 mouse model, but our results suggest that hACE2 may be highly expressed in the mouse brain. Additionally, according to the data provided by the company, these hACE2 mice have abnormal physiology, as indicated by relatively reduced serum triglyceride, cholesterol, and lipase levels, compared to those of wild-type C57BL/6J mice. In summary, our study provides a unique perspective on the pathogenicity of GX_P2V and offers a distinct alternative model for understanding the pathogenic mechanisms of SARS-CoV-2-related coronaviruses.

Lai Wei^{1,#}, Shuiqing Liu^{1,#}, Shanshan Lu^{1,#}, Shengdong Luo², Xiaoping An¹, Huahao

Fan¹, Weiwei Chen², Erguang Li^{3,*}, Yigang Tong^{1,*}, Lihua Song^{1,*}

¹ Beijing Advanced Innovation Center for Soft Matter Science and Engineering, College of Life Science and Technology, Beijing University of Chemical Technology, Beijing, China. ²Research Center for Clinical Medicine, The Fifth Medical Center of PLA General Hospital, Beijing, China. ³State Key Laboratory of Pharmaceutical Biotechnology, Medical School, Nanjing University, China

[#]Contributed equally.

*email: erguang@nju.edu.cn; tong.yigang@gmail.com; songlihua@gmail.com

REFERENCES

1. Liu P, Chen W, Chen JP. Viral Metagenomics Revealed Sendai Virus and Coronavirus Infection of Malayan Pangolins (*Manis javanica*). *Viruses*. 2019 Oct 24;11(11).
2. Lam TT, Jia N, Zhang YW, Shum MH, Jiang JF, Zhu HC, et al. Identifying SARS-CoV-2-related coronaviruses in Malayan pangolins. *Nature*. 2020 Jul;583(7815):282-5.
3. Xiao K, Zhai J, Feng Y, Zhou N, Zhang X, Zou JJ, et al. Isolation of SARS-CoV-2-related coronavirus from Malayan pangolins. *Nature*. 2020 Jul;583(7815):286-9.
4. Huang XY, Chen Q, Sun MX, Zhou HY, Ye Q, Chen W, et al. A pangolin-origin SARS-CoV-2-related coronavirus: infectivity, pathogenicity, and cross-protection by preexisting immunity. *Cell Discov*. 2023 Jun 17;9(1):59.
5. Liu MQ, Lin HF, Li J, Chen Y, Luo Y, Zhang W, et al. A SARS-CoV-2-Related Virus from Malayan Pangolin Causes Lung Infection without Severe Disease in Human ACE2-Transgenic Mice. *J Virol*. 2023 Feb 28;97(2):e0171922.

6. Lu S, Luo S, Liu C, Li M, An X, Li M, et al. Induction of significant neutralizing antibodies against SARS-CoV-2 by a highly attenuated pangolin coronavirus variant with a 104nt deletion at the 3'-UTR. *Emerg Microbes Infect.* 2023 Dec;12(1):2151383.
7. Roberts A, Lamirande EW, Vogel L, Jackson JP, Paddock CD, Guarner J, et al. Animal models and vaccines for SARS-CoV infection. *Virus Res.* 2008 Apr;133(1):20-32.

ACKNOWLEDGEMENTS

This work was supported by NSFC-MFST project (China–Mongolia) (grant number 32161143027), National Key R&D Program of China (2021YFC2301804) and Biosafety Special Program (No. 19SWAQ 13).

ETHICS STATEMENT

All animals involved in this study were housed and cared for in an AAALAC (Association for Assessment and Accreditation of Laboratory Animal Care) accredited facilities. The procedure for animal experiments (IACUC-2019-0027) was approved by the Institutional Animal Care and Use Committee of the Fifth Medical Center, General Hospital of the Chinese People's Liberation Army, and complied with IACUC standards.

AUTHOR CONTRIBUTIONS

L.Song conceived and designed the study and wrote the manuscript. L.W., S.Liu, S.Lu., and S.Luo. performed the experiments and analyzed the data. X.A., H.F., W.C., E.L. and Y.T. analyzed the data and edited the manuscript. L.W. and L.Song wrote the manuscript and all the authors approved the manuscript.

CONFLICT OF INTERESTS

The authors declare no competing interests.

SUPPORTING INFORMATION

Additional Supporting Information for this article can be found online at

DATA AVAILABILITY

All the data supporting the findings of this study are available within the article and the Supporting Information, or from the corresponding author upon reasonable request.

ORCID

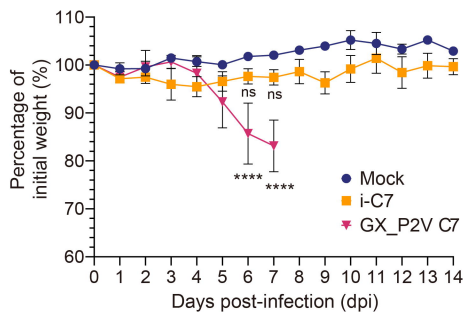
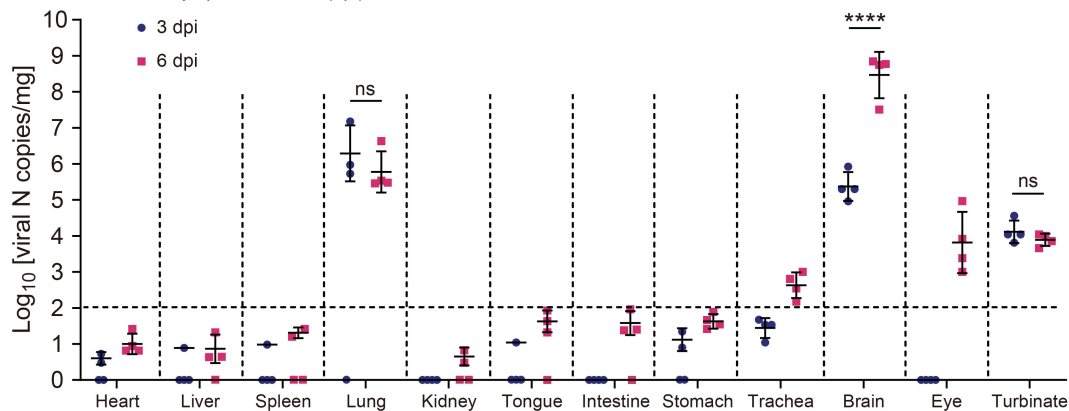
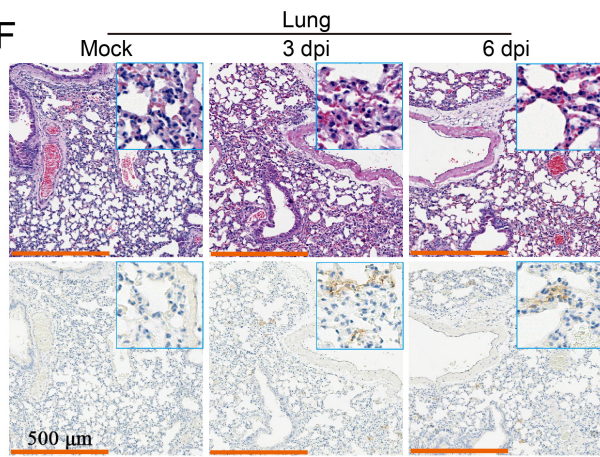
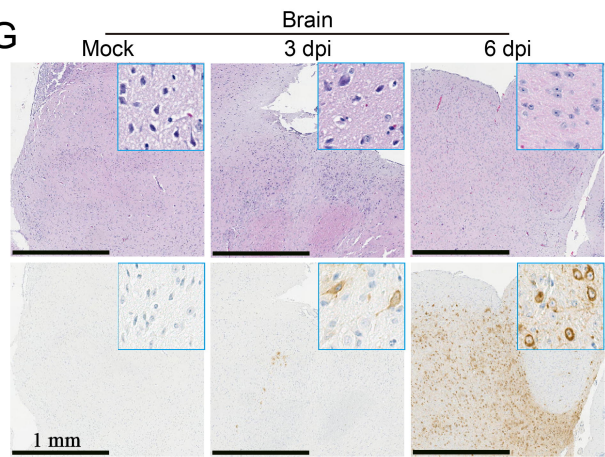
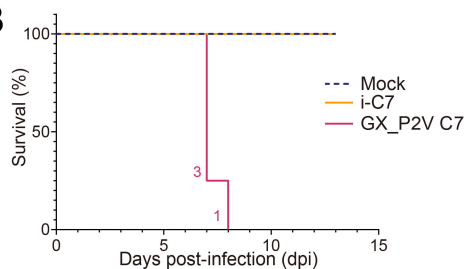
Lihua Song, <https://orcid.org/0000-0002-7299-5719>

Figure 1: Characterization of a lethal infection model in human ACE2-transgenic mice caused by the attenuated SARS-CoV-2-related pangolin coronavirus GX_P2V C7. **A** Mutations in GX_P2V C7 compared to the GX_P2V(short_3UTR) isolate (NCBI accession number: MW532698). The four identical mutations are shown in bold. **B** Survival of hACE2 transgenic mice following intranasal infection with GX_P2V C7 ($n = 4$), inactivated GX_P2V C7 (i-C7, $n = 4$), and mock infection ($n = 4$). The number of deceased mice on each specific day is annotated on the left of the survival curve. **C** Percentage of initial weight of hACE2 transgenic mice after intranasal infection with GX_P2V C7 ($n = 4$), i-C7 ($n = 4$), and mock infection ($n = 4$). The statistical significance of the differences between mock-infected ($n = 4$, blue dots) and GX_P2V C7-infected ($n = 4$, red dots) or i-C7-infected mice ($n = 4$, orange dots) at 6 or 7 dpi are shown. The error bars represent the means \pm SDs. **D** Quantification of GX_P2V N gene copies in heart, liver, spleen, lung, kidney, tongue, intestine, stomach, trachea, brain, eye, and turbinate homogenates at 3- and 6-day post-infection (dpi) ($n = 4$ per group). The limit of detection (LOD) for viral RNA loads in the original samples was $\text{Log}_{10}[10^2 \text{ copies/mg}]$. The error bars represent the means of $\text{Log}_{10}[\text{copies/mg}] \pm$ SDs. The significances of the comparisons in the lung, brain, and turbinate are shown. **E** Infectious viral titers in lung, brain, eye, and turbinate homogenates were measured by plaque forming assay at 3 and 6 dpi ($n = 4$ per group). The statistical significance of the differences in the lung, brain, and turbinate are shown. The error bars represent means of $\text{Log}_{10}[\text{pfu/mL}] \pm$ SDs. **F, G** Hematoxylin and eosin (H&E) staining and immunohistochemical (IHC) staining with an anti-SARS-CoV-2 N-specific antibody

210 (SARS-CoV-2) revealed viral antigen–positive cells (brown) in the lung (**F**) and brain
 211 (**G**), as shown at high magnification in the inset. Scale bars, 500 μm (**F**) and 1 mm (**G**),
 212 respectively. $*P < 0.05$, $**P < 0.01$, $***P < 0.001$, $****P < 0.0001$, $P > 0.05$, not
 213 significant (ns); two-way ANOVA followed by Sidak’s multiple comparison test.

A

Mutation	Codon change	Substitution	CDS Location
1807 A to G	GGA to GGG		ORF1ab
6501 C to U	ACA to AUA	T to I	ORF1ab
19694 C to U	ACA to AUA	T to I	ORF1ab
20930 A to G	GAU to GGU	D to G	ORF1ab
23727 C to U	ACU to AUU	T to I	S
23959 A to C	AAA to AAC	K to N	S
26274 C to A	GCU to GAU	A to D	E
29227 C to U	UAC to UAU		N

C**D****F****G****B****E**